IEEE Access
Multidisciplinary ⋮ Rapid Review ⋮ Open Access Journal

Received April 28, 2022, accepted May 12, 2022, date of publication May 27, 2022, date of current version June 3, 2022.

Digital Object Identifier 10.1109/ACCESS.2022.3178425

Implementation of Exact Linearization Technique for Modeling and Control of DC/DC Converters in Rural PV Microgrid Application

RODRIGO ALIAGA[1], (Student Member, IEEE), MARCO RIVERA[1], (Senior Member, IEEE), PATRICK WHEELER[2], (Fellow, IEEE), JAVIER MUÑOZ[1], (Member, IEEE), JAIME ROHTEN[3], (Member, IEEE), FADIA SEBAALY[4], (Member, IEEE), ARIEL VILLALÓN[1], (Graduate Student Member, IEEE), AND ANDREW TRENTIN[2]

[1]Department of Electrical Engineering, Universidad de Talca, Curicó 3340000, Chile
[2]Department of Electrical and Electronic Engineering, University of Nottingham, Nottingham NG7 2RD, U.K.
[3]Department of Electrical and Electronic Engineering, Universidad del Bío-Bío, Concepción 4051381, Chile
[4]École de Technologie Supérieure, Université de Québec, Montréal, QC H3C 1K3, Canada

Corresponding author: Marco Rivera (marcoriv@utalca.cl)

This work was supported in part by the Agencia Nacional de Investigación y Desarrollo de Chile (ANID), Fondecyt, under Project 1191028; in part by the Fondap Solar Energy Research Center (SERC) Chile under Grant 15110019; in part by the British Embassy in Chile, Fondecyt Regular, under Grant 1220556; and in part by CLIMAT AMSUD under Grant 210001.

ABSTRACT The inclusion of solar systems in rural microgrids is becoming increasingly important to supply energy for irrigation, electric motors, lighting and other. This paper presents the implementation of an exact linearization technique for the modeling and control of a DC/DC converter for use in a microgrid based on a photovoltaic (PV) generation system where non-linear converters are used. The basic advantage of this technique is in linearizing the converter model, thus allowing different operating points to be considered under different conditions. This paper presents a general description of the implemented microgrid topology. The exact linearization theory adapted for power converters is applied to both a Single-Ended Primary-Inductor converter (SEPIC) to extract energy from PV modules and to a Boost converter to increase the voltage. Experimental results are also presented to validate the effectiveness of the proposed control.

INDEX TERMS DC/AC, DC/DC, micro-inverter, renewable energy, rural-microgrid.

I. INTRODUCTION

A microgrid is a system that allows the interconnection of a variety of loads and different electrical sources such as PV, wind and biodiesel. Microgrids can operate either connected to the main electrical grid or isolated. In their operation, robustness must be guaranteed. Considering the nonlinearities of many loads and power converters, they must work under different operating conditions. In this context, the rural-microgrid concept implies the electrification of places where there is no existing access to electricity [1].

There are several control strategies for voltage source converters (VSCs) that may be used in microgrids. The traditional approach is known as voltage-oriented control (VOC) which mainly consists of linear control loops. This gives simple and analytical control synthesis and well-known performance quantification of the control strategy applied. Among those linear control strategies for the inner control of a VSC in a microgrid, PI controllers and hysteresis control may be included [2]. In general, these linear control strategies for VSCs in microgrids have practical limitations. For example the tuning of control parameters are valid only for certain operating points, affecting the microgrid stability under large-signal external disturbances, [3]–[5]. Model-based control strategies appear to be an option to address the previously mentioned limitations. One example of these strategies is predictive control, but these model-based control schemes also have their disadvantages such as the need of knowing the system parameters [6]. Based on this challenge, this work proposes an exact linearization technique [7]–[10] for the control of the power electronic converters used for energy conversion in a microgrid. The benefits of the exact linearization technique are easy implementation, robustness and control stability across with a wide operating range.

The associate editor coordinating the review of this manuscript and approving it for publication was Pinjia Zhang.

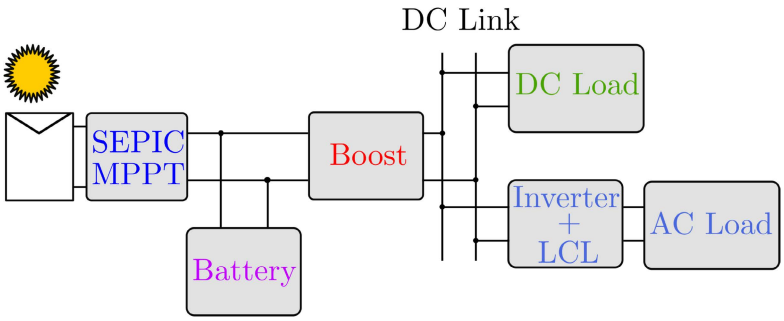

FIGURE 1. Microgrid topology.

The energy source used in this work is solar PV, which implies the use of DC/DC converters to raise or lower the input voltage depending on the case. There are different power converter topologies used in the conversion of PV energy, which can be divided into non-isolated and isolated converters. In the first group there are converters such as Buck, Boost, Cuk, Sepic and Zeta [11]. In the case of isolated converters, the Flyback, Forward, Push Pull, Half-Bridge and Full-Bridge converter [12] can be highlighted. A non-isolated converters use a smaller number of components than isolated converters, which makes them more economical. However, they have a larger size compared to isolated converters [13]. In terms of control, the most important objectives in PV converters are the current and voltage control, maximum power point tracking (MPPT), synchronization with the electrical network, power quality, anti-islanded protection, energy storage and monitoring of PV modules [14]. Regarding the control techniques of the fundamental electrical variables (voltag current), works such as [15]–[18] present the strategies that allow meeting the objective of control and maximization of the use of photovoltaic energy. In this context, works such as [19] describe the use of a voltage-current cascade loop to control the energy extracted and injected into the electrical grid. Reference [20] compares the most used maximum power point tracking algorithms, concluding that the classical methods are more reliable under uniform irradiance conditions, while the intelligent algorithms present a better performance under different irradiance conditions thanks to the increased speed of tracking, sensing and data storage.

The SEPIC and Boost converters can be controlled by the exact linearization technique. The idea behind exact linearization is to redefine the power converter's input as a function of variables and parameters to find a linear relationship between a new input and the output. In this method is not required to consider the dynamics of other variables except those of interest, therefore no reduced model is needed. The linearization can be found by two main ways: input states linearization and input-output linearization. The result obtained with the exact linearization is a transfer function that allows the use of a linear controller such as a simple PI controller, highly simplifying the task of controlling the nonlinear DC/DC converter. In this context, papers such as [7] validate the implementation of the exact linearization technique applied to the control of a Buck-Boost converter. The exact linearization is applicable to PV systems (and other energy sources) [21], where an algorithms is used to track the maximum power point, such as Perturb and Observe (P&O) [22] or Incremental Conductance (IC) [23], [24]. In this implementation, the P&O algorithm is used with a modification, which consists of providing the current as a reference to be followed by the control, instead of the PV module. The novelty of this work is in the application of the exact linearization technique for a SEPIC and Boost converter in a simple and systematic way, obtaining the same models thanks to the generality of the method. Together with the exact linearization, the use of a power balance technique is proposed, with the aim that the converters can operate with different types of loads into the entire power converter's operating region. The final result is reflected in the versatility and robustness of the algorithm for microgrids.

The motivation for the work presented in this paper is to include renewable energy in rural microgrids, where the energy may be required in AC or DC form at different voltage levels (12/24 V and 110/220 V). In the proposed topology indicates that the SEPIC converter charges the battery, tracks the maximum power point (MPP) and supplies the Boost converter. The Boost converter is required increase the voltage to the needed AC level, Figure 1. Additionally, once the DC link voltage is well regulated by the Boost converter, the inverter can be used to supply AC loads. All of the power converters used in this paper are nonlinear, and therefore the control is not necessarily an easy task. Thus, the exact linearization-based control is proposed to be able to manipulate and control the variables in the entire operating region avoiding the intrinsic nonlinearities of these power converters. This paper is organized as follows: Section II provides a general description of the system; Section III details the SEPIC converter model with the linearization process; Section IV presents the boost converter, its linearization, internal and external loop models; Section V details the system stability analysis; Section VI introduces the experimental results; Section VII presents the comparison and finally section VIII concludes this work.

II. SYSTEM DESCRIPTION

A. DESCRIPTION OF THE TOPOLOGY

The general topology is shown in Figure 1, and consists of a SEPIC converter responsible for extracting the energy and storing it in a battery bank. Then, a Boost converter is used to rais the voltage from 12/24 V to a reference voltage for the DC link. Thus, this topology allows the connection of both, DC and AC loads. Finally, by using a full-bridge inverter, the conversion is made to supply AC energy. The inverter [25] output is connected to an LCL [26] filter to obtain a sinusoidal waveform with a lower total harmonic distortion (THD) [27].

The configuration includes two different voltage levels, a low voltage to include typical batteries of 12/24 V, and a higher voltage to be used in the AC voltage 110 V. The proposed control technique is applied to these two power converters (SEPIC and Boost). In both converters similar transfer functions are obtained for the design of the current control loops.

B. INVERTER AND LCL FILTER

An inverter with an LCL filter [28] (Figure 2) was implemented in order to generate the sinusoidal alternating voltage to power single-phase AC loads. Sinusoidal Pulse Width Modulation (SPWM) is used with a switching frequency of 5 kHz, and with a maximum modulation index equal to 1 [29]. In the proposed topology, the Boost converter output voltage is regulated and controlled, for the DC link. The inverter can also be controlled, although it has not been included in this paper [30]–[33]. The switching frequency can be increased to reduce the filter size. However the results given in [34] are adopted and the parameters listed in Table 1 are employed for the AC filter design.

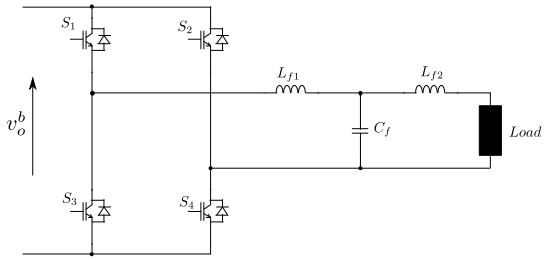

FIGURE 2. Inverter and LCL filter.

III. SEPIC CONVERTER AND MPPT

Figure 3 shows the SEPIC converter topology [35], which is analyzed in this paper. The Single-Ended Primary-Inductor converter has the following characteristics that make it a good choice for extracting energy from PV modules:

- The output voltage can be higher or lower than the input voltage.
- The input current is constant, with slow dynamics related to the weather conditions.
- The capacitor C_s isolates the input from the output, providing some protection against short circuits in the load.

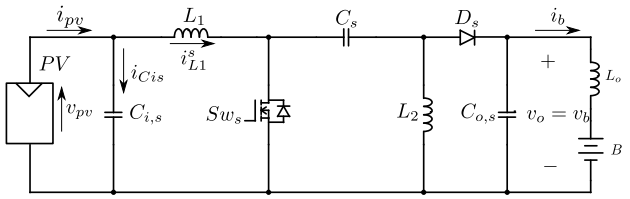

FIGURE 3. SEPIC converter.

The SEPIC converter can reduce or increase the voltage, which allows different voltage levels at the maximum power point of the PV panels. It is therefore possible to connect a high power panel (for example 300 Wp) which has a V_{mpp} over 30 V, or also connect a low power panel (for example 35 Wp) with a V_{mpp} around 17 V.

A. SEPIC CONVERTER MODEL

The SEPIC converter switching states [36] are defined considering both when the switch is closed $Sw_s = 1$ and when the switch is open $Sw_s = 0$. Therefore, the equation that models the current in the inductor for both switch states is:

$$L_1 \frac{di_{L1}^s}{dt} = v_{pv} d_s - v_o(1 - d_s). \tag{1}$$

where d_s is the unifying variable in the SEPIC converter model.

B. SEPIC EXACT LINEARIZATION

Once the equation of the average model for the SEPIC converter has been found, the linearization of the system can proceed. The exact linearization method requires definition of the new inputs variables, in this case the new input variables as u_c^s and u_c^b for the SEPIC and Boost converter, respectively. Between the new inputs and the desired output, the power converter behavior will be linear, as shown in equations (5) and (11).

Considering (1) and defining a new control input for the SEPIC converter, u_c^s as:

$$u_c^s = L_1 \frac{di_{L1}^s}{dt} \tag{2}$$

so:

$$u_c^s = v_{pv} d_s - v_o(1 - d_s). \tag{3}$$

Solving for d_s, the expression of the linearization is obtained.

$$d_s = \frac{u_c^s + v_o}{v_{pv} + v_o}. \tag{4}$$

Applying the Laplace transformation to the equation (2), the following equation can be obtained:

$$H(s) = \frac{i_{L1}^s}{u_c^s} = \frac{1}{sL_1}. \tag{5}$$

This transfer function represents a simple integrator, thus allowing a PI controller to properly follow the reference.

C. CONTROL BLOCK DIAGRAM

As seen above, a linear equivalent plant for the converter can be formed. The general control scheme for the inductor L_1 current is shown in Figure 4(a). Figure 4(b) shows the control block in detail; this is the block that is implemented by the digital controller (STM32), linearizing the current control and generating the trigger signal. u_c^s is the signal that comes from the PI controller and the modulating signal d_s, is obtained from (4). This is compared with the high frequency carrier signal, generating the MOSFETs' control signal in the SEPIC converter.

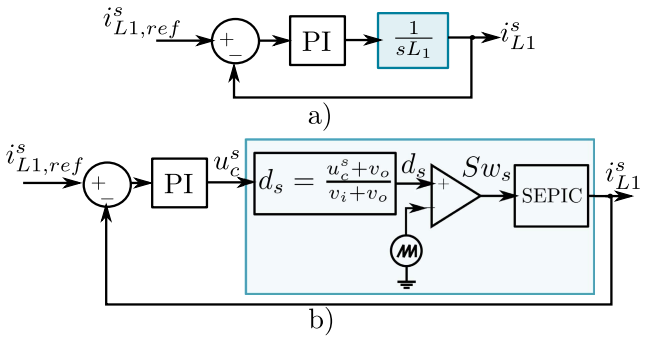

FIGURE 4. Exact linearization, a) simplified-equivalent control block, b) detailed control block.

The linearization process ensures a linear behavior between the new input and the output for every control loop. Small errors on the filter parameter values and sensed variables may lead to minor errors in the controller behavior. Therefore, it is preferred to include an integrator in the controller to ensure zero steady state error and deal with any nonlinear feedback errors. The PI controllers (such as the one chosen in this work) requirements are very low; does not represent a significant cost for the digital processor and includes a integrator which helps to bear these minors errors.

The internal loop corresponds to the current control loop, and must be complement the external one to extract the maximum power from the PV module. To do this, the P&O algorithm is used, which is in charge of delivering the current reference. The implementation of the external loop to track the MPP is detailed below.

D. MPPT AND EXACT LINEARIZATION

In this work, the P&O algorithm is used to track the MPP in the PV curve [22]. The operation principle of the algorithm consists of applying a perturbation to the PV voltage and assessing whether the extracted power of the PV module is higher or lower than the power in the previous sampling time. If it is higher, the algorithm has to track the same path as the power curve; otherwise, it has to change direction. Finally, when the previous power is equal to zero or lower than a small delta of established power, the algorithm has identified the MPP, therefore, P&O will be oscillating around this point until there is a variation in the power curve of the PV module.

The control scheme to extract the energy from the PV modules is shown in Figure 6. The P&O algorithm determines the $i^s_{L1,ref}$ current that must be perturbed to evaluate the power drawn from the PV module. This is possible since the $i^s_{L1,ref}$ current is proportional to the current of the PV module, as shown in Figure 3. The currents according to Kirchhoff's current law are related according to:

$$i_{pv} = i_{Cis} + i^s_{L1,ref}. \tag{6}$$

In steady-state under ideal conditions when no current flows to the capacitor, the currents of the PV module, i_{pv} and the current $i^s_{L1,ref}$, are equal, $i_{pv} = i^s_{L1,ref}$. This justifies the proposed P&O algorithm, which generates the current $i^s_{L1,ref}$ as a reference for the control.

The MPPT algorithm is in charge of finding the exact point of maximum power, i.e., it finds the values of v_{pv} and i_{pv} that maximize the power extraction. However, the MPPT algorithm does not control the SEPIC converter, but only gives the reference to reach the MPP. Therefore, the SEPIC nonlinear based control is in charge of reaching the current reference by manipulating the switching pattern Sw_s, whose algorithm must deal with the dynamics and nonlinearities of the SEPIC converter. Thus, the MPPT algorithm is decoupled with respect the SEPIC nonlinear control, where both of them are required for proper operation.

IV. BOOST CONVERTER

The topology shown in Figure 5 is the non-synchronous Boost converter [37] used in this work. The reason for this choice this topology to raise the voltage is based on demonstrating that the linearization technique can be applied on different converters, the linearization technique makes it easy to use a SEPIC or a Boost converter in the voltage-Boost stage.

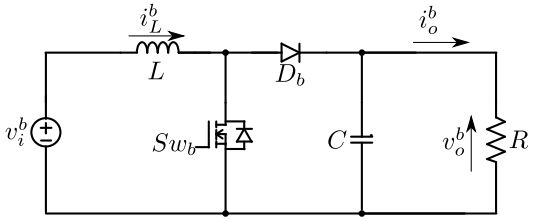

FIGURE 5. Boost converter topology.

A. INTERNAL LOOP TRANSFER FUNCTION

As with the SEPIC converter, the unification equation for the Boost converter is for both states:

$$L\frac{di^b_L}{dt} = v^b_i - v^b_o(1 - d_b). \tag{7}$$

where d_b is the unifying variable in the Boost converter model.

Considering (7) and defining u^b_c as:

$$u^b_c = L\frac{di^b_L}{dt} \tag{8}$$

where:

$$u^b_c = v^b_i - v^b_o(1 - d_b) \tag{9}$$

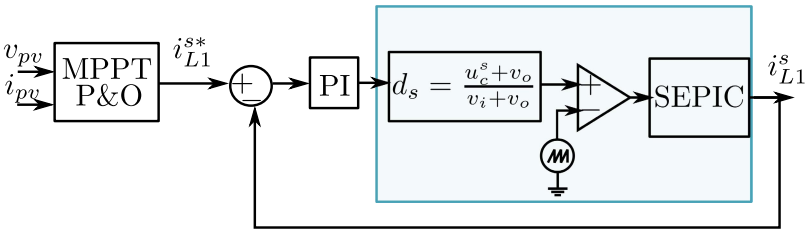

FIGURE 6. SEPIC working with P&O.

then solving for d_b:

$$d_b = 1 + \frac{u_c^b - v_i^b}{v_o^b}. \tag{10}$$

Applying Laplace transforms to (8), the following be obtained:

$$H(s) = \frac{i_L^b}{u_c^b} = \frac{1}{sL}. \tag{11}$$

Equation (10) allows a function for d_b to be obtained, which is compared to the triangular signal, as presented in the control block shown in Figure 8 (a) and (b). A cascade control is shown, with the internal block in charge of controlling the current i_L^b, while the external block is in charge of controlling the output voltage of the Boost converter. This external block generates the reference signal for controlling the current i_L^b. The inner loop is the fast loop and the external loop is slower, by at least a factor of 10.

In this analysis, the modeling of the general system in order to control the output voltage of the Boost converter was been shown. It should be remembered that the output voltage of the Boost converter is the voltage of the DC link, as shown in Figure 1. So the input-output energy balance be used to find a transfer function that allows tuning voltage control in the Boost converter. In real scenarios power converters have an efficiency of less than 100 %. However it is well known that power converter efficiency is high, normally over 96 %. Therefore, the power balancing approximation is not far from reality. Despite the difference between the model and the real implementation being low, PI controllers were employed to ensure proper operation. Finally, to demonstrate that the assumptions are adequate, several experimental tests were performed to validate the systems, as described in section VI.

B. EXTERNAL LOOP TRANSFER FUNCTION

To find the transfer function that represents the Boost converter, the input-output energy balance technique is used. With this transfer function the PI for the external loop of the cascade control can be tuned. The inner loop is the fast loop, which allows the system to establish the equality $I_L^{b*} = i_L^b$ (the reference current is equal to the inductor current L) in steady state.

The fundamental equation of the power balance is presented in Eq. (12):

$$P_i^b = P_o^b. \tag{12}$$

The input power is equal to the input voltage (considered constant for simplicity) multiplied by the input current, which is equal to the current in the inductor L:

$$P_i^b = V_i^b i_L^b \tag{13}$$

and the output power is:

$$P_o^b = \frac{1}{2} C \frac{du_o^b}{dt} + \frac{u_o^b}{R} \tag{14}$$

where:

$$u_o^b = (v_o^b)^2 \tag{15}$$

making equivalent the equations (13) and (14):

$$V_i^b i_L^b = \frac{1}{2} C \frac{du_o^b}{dt} + \frac{u_o^b}{R}. \tag{16}$$

Applying Laplace transformers to (16), the following can be obtained:

$$V_i^b I_L^b(s) = \frac{1}{2} C s U_o^b(s) + \frac{U_o^b(s)}{R}. \tag{17}$$

The previous expression allows finding of the transfer function that relates current i_L^b to voltage $v_{o,ref}^b$:

$$\frac{U_o^b(s)}{I_L^{b*}(s)} = \frac{R V_i^b}{s\left(\frac{RC}{2}\right) + 1}. \tag{18}$$

C. EXTERNAL LINEARIZED PI CONTROL LOOP

Equation (18) shows the transfer function for a fixed resistance. If a load change occurs the control may show inappropriate behavior for extreme impacts. However, the tests in this work were carried out with a model without linearizing (shown in Figure 7) the power balance equation, obtaining correct results for the $R = 200\ \Omega$ with which the plant was tuned and also showing good result with similar load values. To solve this problem the linearization of (16) is implemented, in this way an equivalent plant is obtained equal to:

$$\frac{V_o^b(s)}{I_L^{b*}(s)} = \frac{1}{sC}. \tag{19}$$

Then, considering that the Boost converter output power is equal to:

$$P_o^b = v_o^b i_o^b \tag{20}$$

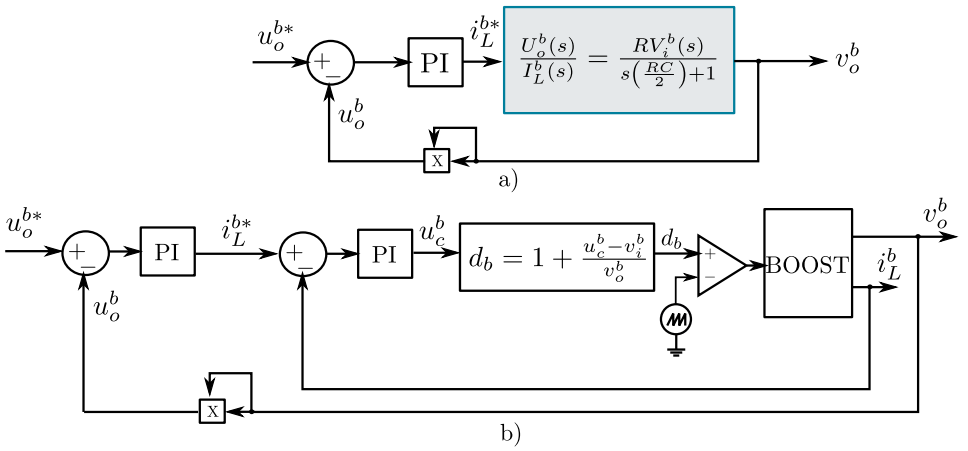

FIGURE 7. Boost converter control block, with internal loop linearized. a) equivalent, b) detailed.

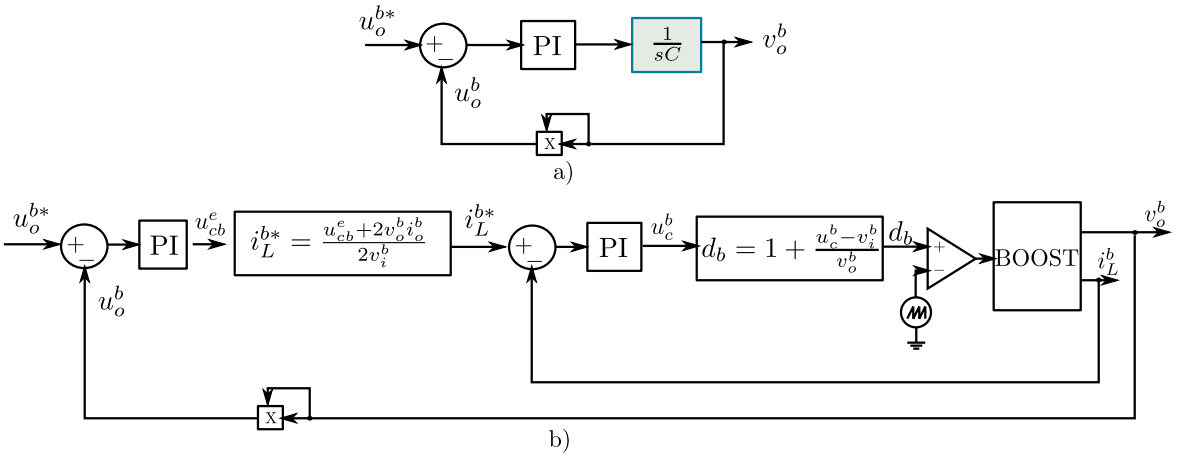

FIGURE 8. Boost converter control block, external and internal loop linearized: a) equivalent, b) detailed.

and solving the derivative of the Eq. (16):

$$C\frac{du_o^b}{dt} = 2\left(V_i^b i_L^b - v_o^b i_o^b\right) \tag{21}$$

defining u_{cb}^e as:

$$u_{cb}^e = C\frac{du_o^b}{dt} \tag{22}$$

replacing:

$$u_{cb}^e = 2\left(v_i^b i_L^b - v_o^b i_o^b\right) \tag{23}$$

solving for i_L^b:

$$i_L^b = \frac{u_{cb}^e + 2v_o^b i_o^b}{2v_i^b}. \tag{24}$$

The block for the control of the voltage base in the energy balance and the exact linearization is shown in Figure 8.

V. STABILITY ANALYSIS

With the selected k_p^{bi} and k_i^{bi} parameters (Table 1), it is possible to address a stability analysis of the proposed linearized system. The direct loop transfer function (25) allows calculation stability margins, as shown in Figure 9.

$$G_b(s) = \frac{k_p^{bi} + \frac{k_i^{bi}}{s}}{sL}. \tag{25}$$

It can be seen that the proposed controller has an infinite gain margin, which ensures the stability regardless of any change in the transfer function gain. Due to the finite value of the phase margin, the convergence of the system will only be compromised if more poles or delays are incorporated into the closed loop. This analysis shows similar results for the SEPIC converter, considering the similarity in the transfer functions obtained after linearization. It is important to note that the aforementioned behavior is valid while the range of the system variables remain within the converter operating region. This is achieved when the duty cycles of both SEPIC and Boost converters are less than one. In order to determine the valid operating range, it is necessary to evaluate the steady state equations of both converters, from where (26) and (27) can be obtained for SEPIC and Boost, respectively.

$$d_s = \frac{v_o}{v_{pv} + v_o} \tag{26}$$

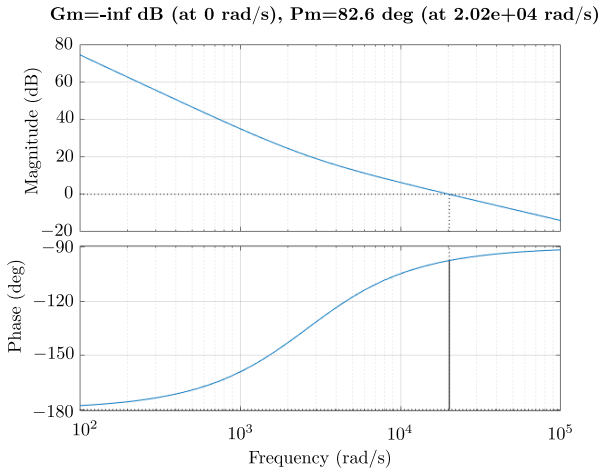

FIGURE 9. Phase margin analysis for the control of the current i_L^b.

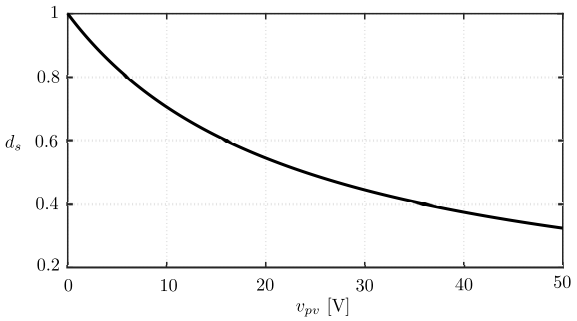

FIGURE 10. SEPIC converter operating range.

$$d_b = \frac{v_o^b - v_i^b}{v_o^b}. \tag{27}$$

Both equations are plotted for different operating values and the curves shown in Figure 10 and Figure 11 can be obtained. It is possible to observe that the only restriction is that the output of the Boost converter must be greater than the battery voltage, which can be ensured with a proper reference. As v_{pv} will always be between zero and the open circuit voltage, the SEPIC converter cannot reach the over modulation region, ensuring linear behavior.

VI. EXPERIMENTAL RESULTS

A. PROTOTYPE IMPLEMENTATION

The experimental setup of the overall microgrid system with the proposed linearization controllers is shown Figure 12. Table 1 shows the system parameters adopted in the implementation. The control is implemented in a STM32 F103C8T6 microcontroller; the frequency of the control interrupt is 10 kHz in the control of the SEPIC and Boost converter, while the switching frequency in both converters is equal to 100 kHz (it is possible to design a smaller filter). Regarding the power involved, there are three PV modules of 300 Wp under STC, one PV module of 35 Wp under STC and three batteries of 12 V / 50 A, to carry out the different tests of the system. The DC bus voltage between

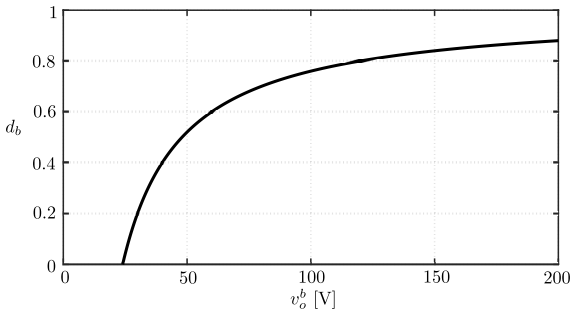

FIGURE 11. Boost converter operating range.

TABLE 1. Setup parameters.

Parameter	Value
$k_p^{s_i}$ (SEPIC converter k_p, internal loop)	19
$k_i^{s_i}$ (SEPIC converter k_i, internal loop)	52000
$k_p^{b_i}$ (Boost converter k_p, internal loop)	19
$k_i^{b_i}$ (Boost converter k_i, internal loop)	52000
$k_p^{b_e}$ (Boost converter k_p, external loop)	0.000347
$k_i^{b_e}$ (Boost converter k_i, external loop)	0.020
L_{f1} (LCL filter input inductance)	2 mH
C_f (LCL capacitor)	1 uF
L_{f2} (LCL filter, output inductance)	1 mH
Maximum power point	300 Wp
V_{oc} (OpenCircuit voltage)	45.17 V
I_{sc} (Short-Circuit current)	8.74 A
V_{mpp} (Max.Power Voltage)	36.72 V
I_{mpp} (Max.Power Current)	8.17 A
$C_{i,s}$ (Input capacitor SEPIC converter)	10000 uF
L_1 (SEPIC converter Inductor)	1 mH
L_2 (SEPIC converter Inductor)	1 mH
C_s (SEPIC converter Capacitor)	4.7 μF
$C_{o,s}$ (SEPIC converter, output capacitor)	470 μF
L (Boost converter inductor)	2 mH
C (Boost converter capacitor)	470 μF

the SEPIC converter and the Boost converter is a function of the battery charge level, and therefore the regulation is due to the battery capacity. Once the battery is fully charged, the SEPIC converter stops sending power to the batteries, protecting them from overcharge.

In the case of the inverter and LCL filter, the technique used to control the semiconductors of the full bridge is not controlled in a closed loop, being the application of a fixed modulator. The Boost converter is in charge of the control of the v_o^b DC voltage, and therefore, the inverter is fed with a regulated voltage and the AC voltage can be defined as $v_{AC}^o = G_{ac} m v_o^b$. Nevertheless, a simple controller can be added to regulate the AC voltage more accurately under different conditions.

All power converters have a limited operating region, which does not always allow overmodulation. Nonlinear based control allows control of the power converter in the entire operating region with a linear behavior, and therefore the natural response of the power converters is improved by this control technique. The proposed system can work properly under any event so long as the power converter remains in the operating region. Naturally, if the event takes the power

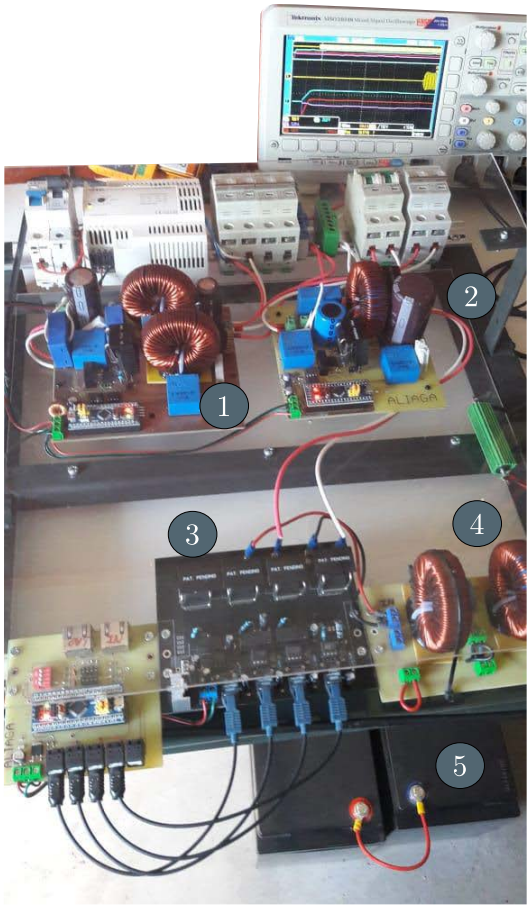

FIGURE 12. Implemented topology: 1) SEPIC, 2) Boost, 3) inverter, 4) LCL filter, 5) battery bank.

converter out of the valid region, there is not sufficient control capable to manage the currents and/or voltages variables to track their respective references. Thus, the proposed control is suitable in the event that the microgrid may fall, as far as the power converter remains in the operating region. Regarding the operating range, this is only limited by conditions of maximum voltage, maximum current, and therefore maximum input power, which are: 50 V, 20 A and 1000 W respectively. The maximum output voltage of the Boost converter was 200 V. It should be mentioned that the control guarantees stability in the full operating range.

The minimum working power of the system is 15 W, therefore, if less than that power is generated, the system trips out, (below that power level, no tests were carried out). In addition, the passive filter and the switching frequency were designed to avoid non-CCM. The main purpose of this work is to evaluate the control technique, it is for this reason that the efficiency of the converters is not evaluated.

The filter parameters can be designed as a function of the transferred power, the switching frequency and the ripple specification on currents and voltages [35], [38]. There are other works that have worked on the filter designed [26], [34] where reference can be made for more details of the approximate selection of the filter components.

B. SEPIC AND MPPT EXPERIMENTAL RESULTS

The implementation of the P&O algorithm was performed with a frequency of 2 Hz, to achieve non-fluctuating dynamics considering the limitations of the P&O algorithm, such as the case presented in [39].

The current disturbance generated by the MPPT algorithm was set equal to 0.2 A for the 300 Wp PV module and 0.05 A for the 35 Wp PV module. The power ripple and the voltage ripple are less than 3%.

1) CASE 1: MPPT TEST

In this case, the P&O algorithm extracts 240 Wp of power from the PV panel. The PV voltage v_{pv} oscillates around 34 V and the current around 8 A values, as it can be seen in Figure 13a. The perturbation of the current is equal to 0.2 A. The time taken to reach the maximum power point is equal to 20 s, considering that the MPPT starts with an extracted power of 150 W.

2) CASE 2: MPPT TEST IN A LOW POWER PV PANEL

In case 2, a low PV power is connected, whose maximum power is 35 Wp under STC. In this case the output voltage is greater than the input, as the result of the connection of two 12 V batteries, adding a total of 24 V. The voltage v_{pv} at the point of maximum power is around 17 V, as shown in Figure 13b, in this image, the current i_{pv}, voltage of the battery bank v_b and the maximum power are detailed. In Figure 13c a zoom of Figure 13b is shown, detailing the disturbance steps in the current i^s_{L1} that are reflected in the current of the PV module, which corresponds to 0.05 A; the frequency of the MPPT as presented in Table 1, is equal to 2 Hz.

3) CASE 3: ELECTRICAL VARIABLES IN BATTERY CHARGING

Figure 13d shows the voltage $v_{pv} = 15$ V, the current $i_{pv} = 1.4$ A and the power $p_{pv} = 21$ W of the PV module. Additionally, the battery voltage $v_b = 26$ V and the current injected into the battery $i_b = 0.75$ A are shown. With these values, the power injected to the battery is equal to 19.5 W which implies, for this case, that the efficiency is equal to 92%.

4) CASE 4: CHANGE OF IRRADIANCE

In this case (Figure 14), a change on the irradiance is applied from 1000 W/m^2 to 900 W/m2. A correct performance is observed in following the maximum power point, from 305 Wp to 275 Wp respectively. The frequency of the P&O algorithm is equal to 10 Hz.

C. EXPERIMENTAL RESULTS FOR THE BOOST CONVERTER

The voltage boost is carried out using a Boost converter. As presented in the analysis, through linearization an easy-to-control plant is obtained in the form of a simple integrator. Therefore, the implementation validates the control strategy proposed in this paper for the voltage boost stage of

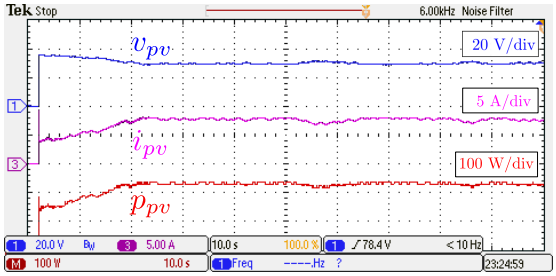

(a) MPPT working extracting a 240 Wp.

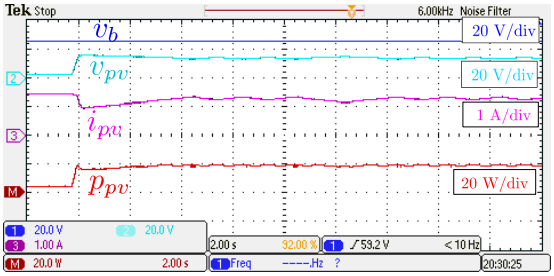

(b) MPPT low power PV.

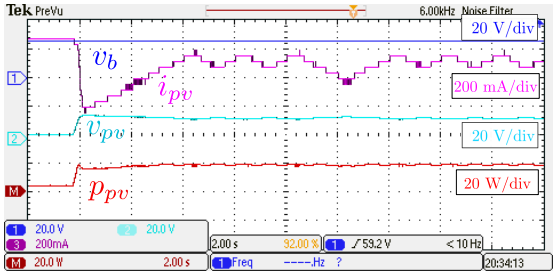

(c) MPPT low power PV, zoom.

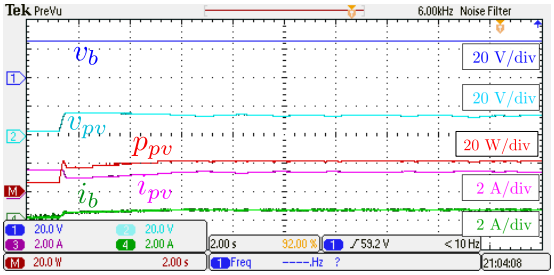

(d) MPPT low power PV and battery injected current.

FIGURE 13. SEPIC converter and MPPT.

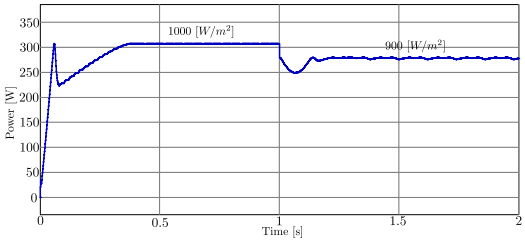

FIGURE 14. Step-change in irradiance from 1000 W/m^2 to 900 W/m^2.

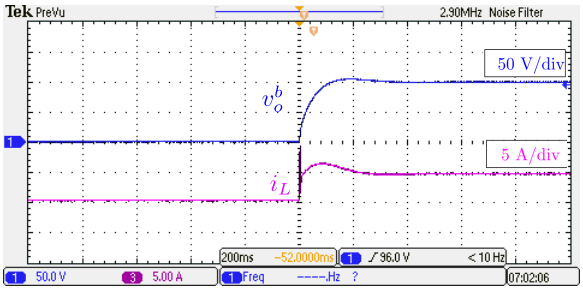

FIGURE 15. Boost converter output 100 V.

the topology. The different control cases are detailed below, either with a load connected to the output of the Boost converter, as well as to the output of the LCL filter after being converted into an AC signal through the full-bridge inverter.

1) CASE 1: CONTROL OF v_o^b, 200 V

In this first case, (Figure 15), the voltage of the Boost converter is controlled at a voltage of 200 V with a load of 200 Ω. The inductor current i_L is observed in the graph; this current is controlled by the internal control loop of the Boost converter and the value of i_L in steady state is equal to 5 A.

2) CASE 2: VOLTAGE STEP CHANGE 50 V, 100 V, AND 150 V

In this case (Figure 16), step changes are made to the output voltage of the Boost converter. The voltages are 50 V, 100 V, and 150 V. The correct performance in the control of the references is observed with a time equal to 300 ms for reaching the steady-state value. In the dynamic and the stationary part of operation, this is a great advantage in a microgrid where loads may require different voltage levels for their operation.

3) CASE 3: AC SIGNAL

Figure 17 shows the output signal of the LCL inverter, with a peak voltage value of 100 V. Figure 18 shows a zoom of the signal, where it can be seen that the control responds properly, independently and very similarly in its response, either if the load is connected to the output of the Boost converter or to the output of the LCL filter. The THD of the AC voltage signal is equal to 1.9 % which represents a value lower than the 5 % established by the IEEE 519-2014 standard.

4) CASE 4: STEP CHANGE AT AC SIGNAL

Finally, in Figure 19, there is a step change from 60 V to 120 V at the output of the Boost converter, and, therefore, the AC signal of the filter takes on these maximum magnitudes.

D. MICROGRID TESTS

The tests carried out are presented with all the power converters working together. Figure 20 shows the voltage, current and power waveforms of the PV module. After 1.6 s the MPPT algorithm is activated, the full-bridge inverter is

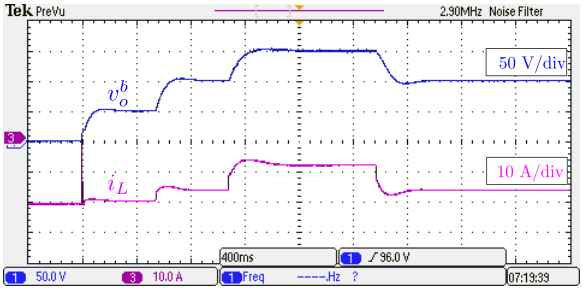

FIGURE 16. Boost converter step ref.

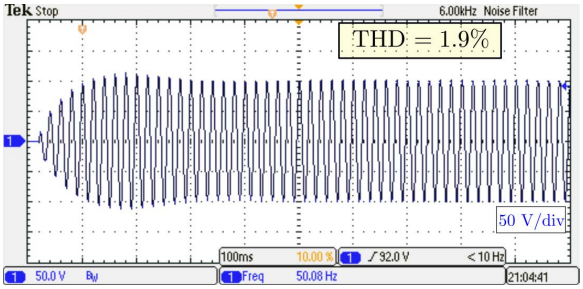

FIGURE 17. AC output voltage.

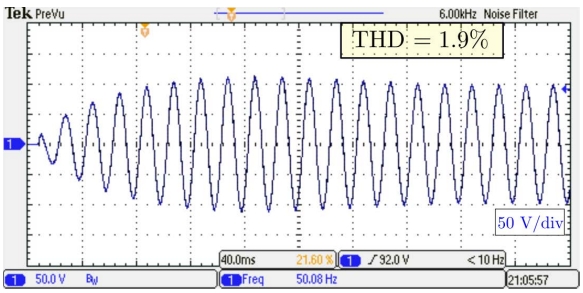

FIGURE 18. Zoom to the output voltage inverter with LCL filter.

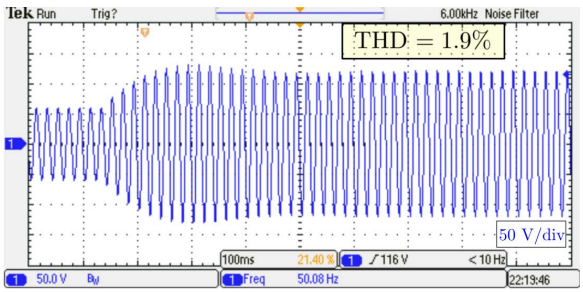

FIGURE 19. Step to the output voltage inverter with LCL filter.

switched-on. It is observed that there are no deficiencies in the general operation of the topology, with power drawn from the PV module in this test of 240 W. Additionally, Figure 21, shows a zoom to the signal presented in Figure 20, where the oscillation of the MPPT (whose current disturbance was set at 0.2 A) and the dynamics of the AC signal at the output of the LCL filter can both be observed. Finally, Figure 22 shows the control around a reference voltage of the Boost converter

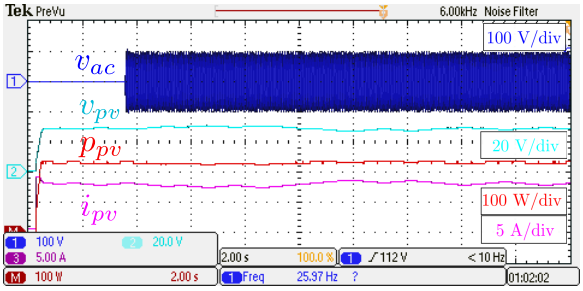

FIGURE 20. MPPT and inverter waveform.

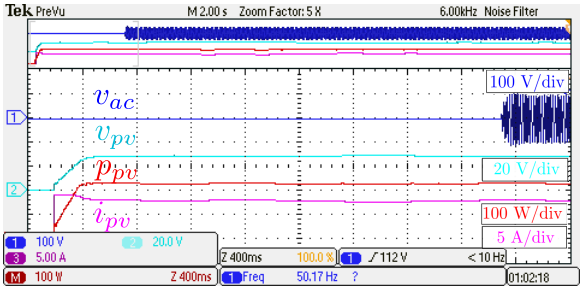

FIGURE 21. MPPT and inverter waveform zoom.

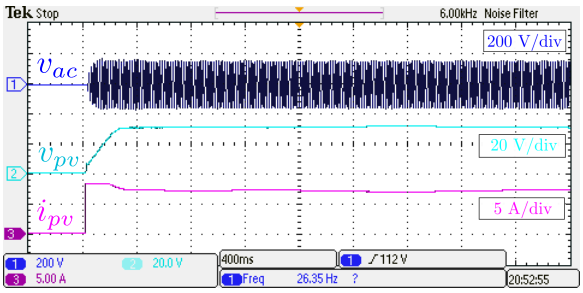

FIGURE 22. MPPT and inverter waveform.

voltage equal to 150 V, next to the graphs of the variables of the PV module.

VII. CONTROL AND TOPOLOGY COMPARISON

A SEPIC converter and a Boost converter have nonlinear behavior, which implies that a linear controller (for example, a PI controller) will have an adequate performance only in the proximity of the operating point where the system was linearized. However, at other values of reference, such a task will not occur. Therefore, strategies that use linear control are not practical for systems that require different operating points, (unless linearized point by point within the operating range, which is impractical). This becomes more impractical in PV systems where the power curve is highly nonlinear. For this reason, the proposed control in this work comes to enhance the controllability of DC-DC converters, whose intrinsic nature is nonlinear. From the point of view of control simplicity, the advantage in the use of exact linearization is clearly appreciated, allowing a simple integrator to be obtained as an equivalent model, unlike the transfer function

TABLE 2. Control strategies disadvantages.

Control	Disadvantages
Predictive control [42]	• Extremely dependent on the parameters of the converters. • High computational cost. • Steady state error.
Fuzzy control [43]	• High computational effort. • There is no mathematical analysis that guarantees that the use of a fuzzy expert system has zero error at steady state.
Hysteresis control [44]	• Variable frequency. • Steady state error.
Neural networks [45]	• Need for a long time of training. • Sensitivity to variables.
Sliding control [46]	• Chaterring

of a SEPIC converter [40] and Boost converter [41] linearized around an operating point. In this way, the design process of a controller that meets the operating requirements of the converters is highly efficient.

In order to justify the superiority of the exact linearization method, Table 2 shows the main disadvantages in other control strategies reported in the literature. In this context, the following comparative points are detailed from Table 2. In the exact linearization technique, there is no extreme dependence on the system parameters, unlike other control strategies, and it can be noted that in both converters in this work, the function of transfer only makes use of the value of the inductance. Regarding the computational effort, only basic mathematical operations are required. For steady state error, it has been shown that this is zero in the exact linearization technique, thanks to the integrator in the transfer function. The switching frequency is fixed, product of comparing a modulating signal with respect to a fixed-frequency triangular. Finally, it is convenient to mention that linearization does not present the disadvantages of fuzzy control, sliding and neural networks.

Regarding the selected topology, the use of a SEPIC converter to extract PV energy has a great advantage over other converters, within the group of non-isolated up and down converters, highlighting that the output voltage is not inverted, and the current input is constant. This last characteristic being a fundamental requirement for the application of the exact linearization technique in converters where the control objective is the current [40].

The SEPIC converter works as a Buck-Boost, thus allowing adequate battery charging independent of their voltage or of the voltage in the PV modules (Figure 13a). In addition, [40] highlights the advantages and characteristics of the SEPIC that make it suitable for charging batteries considering the variable voltage of the PV modules. In this way, this work takes advantage of the research done in [40], immediately using one of the converters that have greater advantages in characteristics such as voltage polarity, input current, switch driver and costs for this application.

In the case of the boost function, as it is only necessary to raise the voltage to standard voltages, a simpler converter such as the Boost converter can be used (Figure 16). This choice allows demonstration that the exact linearization technique is applicable to other topologies using the same methodology for modeling and control.

VIII. CONCLUSION

In this paper, the implementation of an exact linearization technique for control of SEPIC and Boost converters was presented. Such converters are an essential part of a microgrid when one of the energy sources is solar PV. It should be noted that this technique can be applied in different energy conversion systems, including wind and wave energy. The simplification that comes with exact linearization allows the development of simple controllers, with the ability to control the desired variables over a wide range of values to verify the proper performance of the linearization proposal, a prototype was developed with the aforementioned converters, whose objective is the extraction of energy from the PV panels, storage of energy in the battery bank and DC/AC conversion the P&O algorithm and the current control are used, and are able to follow that the reference generated by the MPPT in a proper manner using the current control with exact linearization due to the ability of the SEPIC converter to Boost and Buck the input voltage. It was possible to connect PV panels with a voltage at the maximum power point lower and higher than the battery voltage. The application of exact linearization allows the Boost converter to be controlled even if the voltage rise. DC-type loads, for example some electronic equipment, can be fed directly from the DC link voltage, allowing the size of the inverter operates to be reduced, along with a reduction in losses, increasing the efficiency of the use of energy in a rural-microgrid application.

REFERENCES

[1] M. Nasir, H. A. Khan, A. Hussain, L. Mateen, and N. A. Zaffar, "Solar PV-based scalable DC microgrid for rural electrification in developing regions," *IEEE Trans. Sustain. Energy*, vol. 9, no. 1, pp. 390–399, Jan. 2018.

[2] R. Viswadev, A. Mudlapur, V. V. Ramana, B. Venkatesaperumal, and S. Mishra, "A novel AC current sensorless hysteresis control for grid-tie inverters," *IEEE Trans. Circuits Syst. II, Exp. Briefs*, vol. 67, no. 11, pp. 2577–2581, Nov. 2020.

[3] J. Rocabert, A. Luna, F. Blaabjerg, and P. Rodríguez, "Control of power converters in AC microgrids," *IEEE Trans. Power Electron.*, vol. 27, no. 11, pp. 4734–4749, Nov. 2012.

[4] M. Ahmed, L. Meegahapola, A. Vahidnia, and M. Datta, "Stability and control aspects of microgrid architectures–A comprehensive review," *IEEE Access*, vol. 8, pp. 144730–144766, 2020.

[5] T. Dragicevic, S. Vazquez, and P. Wheeler, "Advanced control methods for power converters in DG systems and microgrids," *IEEE Trans. Ind. Electron.*, vol. 68, no. 7, pp. 5847–5862, Jul. 2021.

[6] M. Khosravi, M. Amirbande, D. A. Khaburi, M. Rivera, J. Riveros, J. Rodriguez, A. Vahedi, and P. Wheeler, "Review of model predictive control strategies for matrix converters," *IET Power Electron.*, vol. 12, no. 12, pp. 3021–3032, Oct. 2019.

[7] L. Callegaro, M. Ciobotaru, D. J. Pagano, and J. E. Fletcher, "Feedback linearization control in photovoltaic module integrated converters," *IEEE Trans. Power Electron.*, vol. 34, no. 7, pp. 6876–6889, Jul. 2019.
[8] C. R. Baier, M. A. Torres, P. Acuna, J. A. Muñoz, P. E. Melín, C. Restrepo, and J. I. Guzman, "Analysis and design of a control strategy for tracking sinusoidal references in single-phase grid-connected current-source inverters," *IEEE Trans. Power Electron.*, vol. 33, no. 1, pp. 819–832, Jan. 2018.
[9] J. Zhou and X. Lu, "Review of exact linearization method applied to power electronics system," in *Proc. Asia–Pacific Power Energy Eng. Conf.*, Mar. 2012, pp. 1–4.
[10] W. E. Aouni and L.-A. Dessaint, "Real-time implementation of input-state linearization and model predictive control for robust voltage regulation of a DC-DC boost converter," *IEEE Access*, vol. 8, pp. 192101–192108, 2020.
[11] X.-F. Cheng, C. Liu, D. Wang, and Y. Zhang, "State-of-the-Art review on soft-switching technologies for non-isolated DC-DC converters," *IEEE Access*, vol. 9, pp. 119235–119249, 2021.
[12] X. Pan, H. Li, Y. Liu, T. Zhao, C. Ju, and A. K. Rathore, "An overview and comprehensive comparative evaluation of current-fed-isolated-bidirectional DC/DC converter," *IEEE Trans. Power Electron.*, vol. 35, no. 3, pp. 2737–2763, Mar. 2020.
[13] F. Blaabjerg, "*Control of Power Electronic Converters and Systems*, vol. 1. New York, NY, USA: Academic, 2018.
[14] D. Murillo-Yarce, J. Alarcón-Alarcón, M. Rivera, C. Restrepo, J. Muñoz, C. Baier, and P. Wheeler, "A review of control techniques in photovoltaic systems," *Sustainability*, vol. 12, no. 24, p. 10598, Dec. 2020.
[15] R.-J. Wai and W.-H. Wang, "Grid-connected photovoltaic generation system," *IEEE Trans. Circuits Syst. I, Reg. Papers*, vol. 55, no. 3, pp. 953–964, Apr. 2008.
[16] A. Merabet, L. Labib, A. M. Y. M. Ghias, C. Ghenai, and T. Salameh, "Robust feedback linearizing control with sliding mode compensation for a grid-connected photovoltaic inverter system under unbalanced grid voltages," *IEEE J. Photovolt.*, vol. 7, no. 3, pp. 828–838, May 2017.
[17] M. B. Shadmand, R. S. Balog, and H. Abu-Rub, "Model predictive control of PV sources in a smart DC distribution system: Maximum power point tracking and droop control," *IEEE Trans. Energy Convers.*, vol. 29, no. 4, pp. 913–921, Dec. 2014.
[18] J. Hong, J. Yin, Y. Liu, J. Peng, and H. Jiang, "Energy management and control strategy of photovoltaic/battery hybrid distributed power generation systems with an integrated three-port power converter," *IEEE Access*, vol. 7, pp. 82838–82847, 2019.
[19] L. V. Bellinaso, H. H. Figueira, M. F. Basquera, R. P. Vieira, H. A. Grundling, and L. Michels, "Cascade control with adaptive voltage controller applied to photovoltaic boost converters," *IEEE Trans. Ind. Appl.*, vol. 55, no. 2, pp. 1903–1912, Mar. 2019.
[20] R. B. Bollipo, S. Mikkili, and P. K. Bonthagorla, "Hybrid, optimal, intelligent and classical PV MPPT techniques: A review," *CSEE J. Power Energy Syst.*, vol. 7, no. 1, pp. 9–33, Jan. 2021.
[21] C. R. Baier, M. Torres, J. A. Muñoz, R. A. Marco, E. N. Eduardo, and P. Acuña, "Bidirectional power flow control of a single-phase current-source grid-tie battery energy storage system," in *Proc. IEEE 24th Int. Symp. Ind. Electron. (ISIE)*, Jun. 2015, pp. 1372–1377.
[22] D. Sera, L. Mathe, T. Kerekes, S. V. Spataru, and R. Teodorescu, "On the perturb-and-observe and incremental conductance MPPT methods for PV systems," *IEEE J. Photovolt.*, vol. 3, no. 3, pp. 1070–1078, Jul. 2013.
[23] K. Jain, M. Gupta, and A. K. Bohre, "Implementation and comparative analysis of P&O and INC MPPT method for PV system," in *Proc. 8th IEEE India Int. Conf. Power Electron. (IICPE)*, Dec. 2018, pp. 1–6.
[24] S. Bhattacharyya, D. S. Kumar P, S. Samanta, and S. Mishra, "Steady output and fast tracking MPPT (SOFT-MPPT) for P&O and InC algorithms," *IEEE Trans. Sustain. Energy*, vol. 12, no. 1, pp. 293–302, Jan. 2021.
[25] M. Pokharel, N. Hildebrandt, C. N. M. Ho, and Y. He, "A fast-dynamic unipolar switching control scheme for single-phase inverters in DC microgrids," *IEEE Trans. Power Electron.*, vol. 34, no. 1, pp. 916–927, Jan. 2019.
[26] F. Li, X. Zhang, H. Zhu, H. Li, and C. Yu, "An LCL-LC filter for grid-connected converter: Topology, parameter, and analysis," *IEEE Trans. Power Electron.*, vol. 30, no. 9, pp. 5067–5077, Sep. 2015.
[27] *IEEE Recommended Practice and Requirements for Harmonic Control in Electric Power Systems*, IEEE Standard 519-2014 (Revision IEEE Standard 519-1992), 2014, pp. 1–29.
[28] Y. Tang, W. Yao, P. C. Loh, and F. Blaabjerg, "Design of *LCL* filters with *LCL* resonance frequencies beyond the Nyquist frequency for grid-connected converters," *IEEE Trans. Emerg. Sel. Topics Power Electron.*, vol. 4, no. 1, pp. 3–14, Mar. 2016.
[29] M. Lakka, E. Koutroulis, and A. Dollas, "Development of an FPGA-based SPWM generator for high switching frequency DC/AC inverters," *IEEE Trans. Power Electron.*, vol. 29, no. 1, pp. 356–365, Jan. 2014.
[30] D. Puyal, L. A. Barragan, J. Acero, J. M. Burdio, and I. Millan, "An FPGA-based digital modulator for full- or half-bridge inverter control," *IEEE Trans. Power Electron.*, vol. 21, no. 5, pp. 1479–1483, Sep. 2006.
[31] W. J. Cha, J. M. Kwon, and B. H. Kwon, "Highly efficient asymmetrical PWM full-bridge converter for renewable energy sources," *IEEE Trans. Ind. Electron.*, vol. 63, no. 5, pp. 2945–2953, May 2016.
[32] D. Wu, Y. Wu, J. Kan, Y. Tang, J. Chen, and L. Jiang, "Full-bridge current-fed PV microinverter with DLFCR reduction ability," *IEEE Trans. Power Electron.*, vol. 35, no. 9, pp. 9541–9552, Sep. 2020.
[33] M. Ciobotaru, R. Teodorescu, and F. Blaabjerg, "Control of single-stage single-phase PV inverter," in *Proc. Eur. Conf. Power Electron. Appl.*, 2005, p. 10.
[34] M. Sanatkar-Chayjani and M. Monfared, "Design of LCL and LLCL filters for single-phase grid connected converters," *IET Power Electron.*, vol. 9, no. 9, pp. 1971–1978, Jul. 2016.
[35] J. J. Jozwik and M. K. Kazimierczuk, "Dual SEPIC PWM switching-mode DC/DC power converter," *IEEE Trans. Ind. Electron.*, vol. 36, no. 1, pp. 64–70, Feb. 1989.
[36] E. Babaei and M. E. S. Mahmoodieh, "Calculation of output voltage ripple and design considerations of SEPIC converter," *IEEE Trans. Ind. Electron.*, vol. 61, no. 3, pp. 1213–1222, Mar. 2014.
[37] M. Forouzesh, P. Y. Siwakoti, A. S. Gorji, F. Blaabjerg, and B. Lehman, "Step-up DC-DC Converters: A comprehensive review of voltage-boosting techniques, topologies, and applications," *IEEE Trans. Power Electron.*, vol. 32, no. 12, pp. 9143–9178, Dec. 2017.
[38] S. A. Shirsavar, "Teaching practical design of switch-mode power supplies," *IEEE Trans. Educ.*, vol. 47, no. 4, pp. 467–473, Nov. 2004.
[39] C. González-Castaño, C. Restrepo, S. Kouro, and J. Rodriguez, "MPPT algorithm based on artificial bee colony for PV system," *IEEE Access*, vol. 9, pp. 43121–43133, 2021.
[40] S. J. Chiang, H.-J. Shieh, and M.-C. Chen, "Modeling and control of PV charger system with SEPIC converter," *IEEE Trans. Ind. Electron.*, vol. 56, no. 11, pp. 4344–4353, Nov. 2009.
[41] R. H. G. Tan and L. Y. H. Hoo, "DC-DC converter modeling and simulation using state space approach," in *Proc. IEEE Conf. Energy Convers. (CENCON)*, Oct. 2015, pp. 42–47.
[42] M. Khalilzadeh, S. Vaez-Zadeh, J. Rodriguez, and R. Heydari, "Model-free predictive control of motor drives and power converters: A review," *IEEE Access*, vol. 9, pp. 105733–105747, 2021.
[43] P. Mattavelli, L. Rossetto, G. Spiazzi, and P. Tenti, "General-purpose fuzzy controller for DC-DC converters," *IEEE Trans. Power Electron.*, vol. 12, no. 1, pp. 79–86, Jan. 1997.
[44] T. Xue and H. Cheng, "Research and improvement of current hysteresis control strategy for boost DC-DC converter," in *Proc. Int. Conf. Sensor Netw. Signal Process. (SNSP)*, Oct. 2018, pp. 266–270.
[45] N. Chettibi, A. Mellit, G. Sulligoi, and A. M. Pavan, "Adaptive neural network-based control of a hybrid AC/DC microgrid," *IEEE Trans. Smart Grid*, vol. 9, no. 3, pp. 1667–1679, May 2018.
[46] R.-J. Wai and L.-C. Shih, "Design of voltage tracking control for DC–DC boost converter via total sliding-mode technique," *IEEE Trans. Ind. Electron.*, vol. 58, no. 6, pp. 2502–2511, Jun. 2011.